ELSEVIER

Journal of Alloys and Compounds 228 (1995) 16–22

Journal of ALLOYS AND COMPOUNDS

Crystal structure and physical properties of $Ce_3Pd_6Sb_5$

R.A. Gordon[a], F.J. DiSalvo[a,*], R. Pöttgen[b]

[a]*Department of Chemistry, Cornell University, Ithaca, NY 14853, USA*
[b]*Max-Planck-Institut für Festkörperforschung Heisenbergstrasse 1, D-70569 Stuttgart, Germany*

Received 20 February 1995; in final form 24 April 1995

Abstract

A new ternary antimonide, $Ce_3Pd_6Sb_5$, was prepared by arc melting of the elemental components and subsequent annealing at 750 °C. Its orthorhombic crystal structure was determined from single-crystal X-ray data: space group, *Pmmn*; $Z = 2$; $a = 1348.1(2)$ pm, $b = 445.9(1)$ pm and $c = 1005.0(1)$ pm; $V = 0.6041(2)$ nm^3, $wR_2 = 0.045$; 1432 F^2 values; 48 variables. The structure of $Ce_3Pd_6Sb_5$ is of a new type, built from three pseudo-body-centered subcells of the cerium atoms. Palladium and antimony atoms form a three-dimensional infinite polyanion $[Pd_6Sb_5]$ with an atomic arrangement derived from the well-known $ThCr_2Si_2$ and $CaBe_2Ge_2$ structures. The crystal chemistry of this new compound is discussed together with the related $Dy_3Co_6Sn_5$-type structure. The magnetic susceptibility exhibits significant anisotropy with an effective high temperature moment per cerium of 2.67 μ_B and antiferromagnetic ordering at 6 K. The resistance shows a minimum near 17 K, possibly suggesting some Kondo-type interactions, and an anomaly at 6 K which corresponds to the antiferromagnetic ordering.

Keywords: Physical properties; Crystal structure; Magnetic susceptibility

1. Introduction

In most rare-earth intermetallics, 4f electrons are expected to be well localized compared with d electrons in transition metal compounds and 5f electrons in actinide intermetallics. However, 4f electrons in cerium-based intermetallics are subject to crystal field effects (CEF) and occasionally extensive hybridization with conduction electrons. This hybridization can lead to an instability of the localized state and results in a wide variety of unusual magnetic and electrical properties such as intermediate valence, where the effective cerium moment lies between trivalence and tetravalence, or heavy-fermion behavior, where a strong Kondo interaction leads to a high effective mass for conduction electrons [1–3].

In the course of our systematic studies of cerium intermetallics [4–6], we investigated the ternary system cerium–palladium–antimony. Three other phases are currently known in the Ce–Pd–Sb system: CePdSb, a ferromagnetic Kondo lattice system [7–9], $CePd_2Sb_2$ [10] and the recently reported $CePdSb_2$ [11]. No properties have yet been reported for $CePd_2Sb_2$ [12], while magnetic data on $CePdSb_2$ suggests antiferromagnetic behavior [11]. Given that $CePd_3$ is one of the most unusual intermediate valence materials [13,14], we hope that, by searching the palladium-rich region of the Ce–Pd–Sb ternary system, we may find materials that exhibit interesting electronic effects. Our preliminary investigations have produced a new ternary, $Ce_3Pd_6Sb_5$. Herein, we discuss the structural characteristics, resistance and magnetic susceptibility from 4.2 K to 300 K.

2. Experimental

Elements of at least 99.9% purity (Ce ingot, Sb shot, Cerac Inc.; Pd wire of 1 mm diameter, Strem) were used in sample preparation. The cerium was first melted under vacuum and allowed to drip into a water-cooled copper cup. This was done for ease of cutting with heavy-wire cutters and helped to reduce ferromagnetic impurities that are often present after sawing Ce into pieces. Arc melting was

* Corresponding author.

0925-8388/95/$09.50 © 1995 Elsevier Science S.A. All rights reserved
SSDI 0925-8388(95)01689-9

performed under flowing argon, gettered in a titanium purifier (Centorr Furnaces model 2B-20) on a tantalum-coated water-cooled copper hearth. Owing to the significant vapour pressure of antimony at elevated temperatures, a small excess (about 3%) was included. Samples were turned over and melted at least three times to ensure homogeneity. Sample masses after arc melting were within 0.5% of the stoichiometric values (assuming all loss to be Sb). Initially, a sample of composition "$CePd_3Sb_2$" was prepared. it was placed in a section of tantalum tubing and sealed under vacuum in a quartz tube for a 2 week anneal treatment at 750 °C. This sample underwent slight partial melting while annealing. Crystals were quite evident when the sample was broken apart. Initial crystal structure refinement work gave a composition of $Ce_3Pd_6Sb_5$. Microprobe analysis on an unpolished portion of the sample using a JEOL 733 scanning electron microscope and CePdSb as a standard suggested a composition of 21(2) at.% Ce, 45(2) at.% Pd and 34(2) at.% Sb, in agreement with the initial refinement. Further samples were prepared at the correct stoichiometry for measurement. The melted and annealed buttons are light grey and stable in air. They are brittle and, after anneal, exhibit small fractures both on the surface and inside the buttons. While $Ce_3Pd_6Sb_5$ powder is dark grey, single crystals of $Ce_3Pd_6Sb_5$ exhibit a metallic lustre.

The samples were characterized through their powder diffraction patterns collected on both a Scintag θ–2θ diffractometer and a Guinier camera using Cu $K\alpha_1$ radiation and silicon of 99.999% points (a = 543.07 pm) as an internal standard. The patterns were analyzed using the program TREOR [15] and the cell constants obtained thereby were refined by a least-squares technique.

Single-crystal intensity data were collected on a four-circle diffractometer (CAD4) with graphite-monochromatized Ag Kα radiation and a scintillation counter with pulse height discrimination. Crystals examined were from the "$CePd_3Sb_2$" sample. Using the LAZY-PULVERIX program [16], a theoretical powder pattern was calculated on the basis of positional parameters of the refined structure for comparison with the observed powder pattern.

Magnetic measurements were performed between 4.2 and 300 K by the Faraday technique on loose ground material and analyzed as described elsewhere [4]. Four-probe resistance meaurements between 4.2 and 300 K were performed on an ingot roughly 1.4 mm × 4 mm × 8.5 mm cut with a string saw from a larger button. The presence of microcracks in the sample prevented the determination of absolute resistivity.

3. Results and discussion

3.1. Crystal structure

Very-well-shaped single crystals of $Ce_3Pd_6Sb_5$ were isolated from a crushed button of an intended composition "$CePd_3Sb_2$" after the annealing process. Burgers precession photographs were taken in order to establish both their symmetry and suitability for intensity data collection. They showed the high orthorhombic Lauë symmetry *mmm*, and the systematic extinctions (*hk*0 only observed with $h + k = 2n$) led to the space groups *Pmmn*, $P2_1mn$ and $Pm2_1n$, of which the centrosymmetric group *Pmmn* (No. 59) was found to be correct during structure refinement. Crystallographic data and details of the data collection are summarized in Table 1.

The starting atomic parameters were deduced from an interpretation of direct methods [17] and the structure was then successfully refined using SHELXL-93 [18] with anisotropic displacement parameters for all atoms. A final difference Fourier syntheses revealed no significant residual peaks (all between +4 and −2 electrons $Å^{-3}$). The refined atomic parameters and the interatomic distances are listed in Tables 2 and 3. A comparison of calculated intensities with observed ones from powder data on $Ce_3Pd_6Sb_5$ is contained in Table 4.

The structure of $Ce_3Pd_6Sb_5$ is a new type. Although its composition is close to 1:2:2, only parts of the structure are related to the well-known $ThCr_2Si_2$ [19] and $CaBe_2Ge_2$ [20] structure types.

A projection of the $Ce_3Pd_6Sb_5$ structure together with coordination polyhedra is shown in Fig. 1. The structure of $Ce_3Pd_6Sb_5$ is built up from three pseudo-body-centered subcells formed by the cerium atoms. In analogy to the $ThCr_2Si_2$ and $CaBe_2Ge_2$ structures, the palladium and antimony atoms form a three-dimensional infinite network, as shown in Fig. 2.

The topological relationship between the prototypes $ThCr_2Si_2$ and $CaBe_2Ge_2$ and the defect versions of composition 3:6:5 are shown in Fig. 3. For $CaBe_2Ge_2$ and $Ce_3Pd_6Sb_5$, the origins of the unit cells are shifted for better comparison with the other structures. In $ThCr_2Si_2$ and $CaBe_2Ge_2$, the $[Cr_2Si_2]$ and $[Be_2Ge_2]$ polyanionic networks are highly symmetrical. The silicon atoms in $ThCr_2Si_2$ form pairs, whereas no Ge–Ge contacts occur in $CaBe_2Ge_2$. This same paired and unpaired relation exists between $Dy_3Co_6Sn_5$ [22,23] and $Ce_3Pd_6Sb_5$. The Sn(2) atoms in the dysprosium cobalt stannide form pairs at a distance of 303 pm [22]. In contrast, there is no strong antimony–antimony bonding in $Ce_3Pd_6Sb_5$. The shortest Sb–Sb distance (Sb(1)–Sb(1)) is at 340.5 pm, somewhat larger than twice the metallic radius of antimony,

Table 1
Crystal data and structure refinement for $Ce_3Pd_6Sb_5$

Empirical formula	$Ce_3Pd_6Sb_5$
Formula weight (g mol^{-1})	1667.5
Temperature (K)	293(2)
Wavelength (pm)	56.087
Crystal system	Orthorhombic
Space group	*Pmmn* (No. 59)
Unit-cell dimensions	
a (pm)	1348.1(2)
b (pm)	445.9(1)
c (pm)	1005.0(1)
V (nm^3)	0.6041(2)
Formula units per cell Z	2
Calculated density (Mg m^{-3})	9.167
Crystal size (μm × μm × μm)	30 × 30 × 125
Absorption correction	From ψ scan data
Transmission ratio (maximum:minimum)	1:0.908
Absorption coefficient (mm^{-1})	16.2
F(000)	1410
θ range for data collection (°)	2–28
Scan mode	ω–θ
Range in hkl	$-22 \leq h \leq 22, 0 \leq k \leq 6, -15 \leq l \leq 16$
Total number of reflections	4824
Number of independent reflections	1433 (R_{int} = 0.0264)
Refinement method	Full-matrix least-squares on F^2
Number of data	1432
restraints	0
parameters	48
Goodness of fit on F^2	1.192
Final R indices [$(I > 2\sigma(I))$]	0.0197
R_1	0.0436
R indices (all data)	0.0219
wR_2	0.0446
Extinction coefficient	0.0029(1)
Largest difference peak and hole (electrons nm^{-3})	4002 and −2144

Table 2
Atomic coordinates and isotropic displacement parameters for $Ce_3Pd_6Sb_5$

Atom	Wyckoff site	x	y	z	U_{eq}[a] (pm^2)
Ce(1)	2a	1/4	1/4	0.75756(3)	84(1)
Ce(2)	4f	0.57480(2)	1/4	0.75467(2)	78(1)
Pd(1)	4f	0.41109(3)	1/4	0.00819(4)	122(1)
Pd(2)	2b	1/4	3/4	0.01545(5)	125(1)
Pd(3)	4f	0.56761(3)	1/4	0.39730(4)	136(1)
Pd(4)	2b	1/4	3/4	0.47745(6)	150(1)
Sb(1)	4f	0.37627(2)	1/4	0.47697(3)	111(1)
Sb(2)	4f	0.58653(2)	1/4	0.13700(3)	91(1)
Sb(3)	2a	1/4	1/4	0.16899(5)	115(1)

[a] U_{eq} is defined as one third of the trace of the orthogonalized U_{ij} tensor.

318 pm, in a 12-coordinated (coordination number (CN) 12) environment [24].

The $[Co_6Sn_5]$ network in $Dy_3Co_6Sn_5$ is more symmetrical than the $[Pd_6Sb_5]$ network in $Ce_3Pd_6Sn_5$. This is certainly portended by the higher symmetry space group (*Immm*) of $Dy_3Co_6Sn_5$. While the structure of $Dy_3Co_6Sn_5$ is derived from the $ThCr_2Si_2$ type, $Ce_3Pd_6Sb_5$ is more closely related to the $CaBe_2Ge_2$ type (*P4/nmm*). The *n* glide plane of the tetragonal structure is preserved in the tripled cell of $Ce_3Pd_6Sb_5$. In examining Fig. 3, one can envison $Dy_3Co_6Sn_5$ as three $ThCr_2Si_2$-type cells (tripled along ***b***) from which an Sn atom has been removed from the outside ($y = 0$) and Sn atoms at $y = 0.5$ have moved to $z = 0$, causing the second Sn absence (two formula units per orthorhombic cell). The $Ce_3Pd_6Sb_5$ cell can be viewed as three $CaBe_2Ge_2$-type cells (tripled along ***a***) from which Sb atoms have been removed from the outside ($x = 0$) and the lower centre ($x = 0.5$) of the cell shown in Fig. 3.

Defect $CaBe_2Ge_2$ and $ThCr_2Si_2$ structures with transition element defects have been observed in rare earth–nickel pnictides [25], for $CeNi_{2-x}Sb_2$ in particular, but not necessarily with pnictogen defects. Indeed, an orthorhombic distortion has also been reported [26] for a composition $CeNi_{2.35}Sb_{1.65}$ ($CeNi_{2.35-x}Sb_{1.65}$ based on [25]) but, unlike $Ce_3Pd_6Sb_5$, no tripled ***a*** was observed.

The structure of $Ce_3Pd_6Sb_5$ has two crystallographically different cerium positions. They have the high

Table 3
Interatomic distances in the structure of $Ce_3Pd_6Sb_5$[a]

Atoms	Interatomic distance (pm)	Atoms	Interatomic distance (pm)	Atoms	Interatomic distance (pm)
Ce(1)–2Sb(1)	329.4	Pd1–2Sb(2)	266.5	Sb1–2Pd(3)	267.2
4Sb(2)	330.9	1Sb(2)	269.6	1Pd(3)	270.1
2Pd(1)	332.6	1Sb(3)	270.7	2Pd(4)	280.5
2Pd(2)	341.9	2Pd(2)	311.3	2Ce(2)	329.0
2Pd(4)	359.1	2Ce(2)	326.9	1Ce(1)	329.4
4Pd(3)	366.6	2Pd(1)	327.8	1Sb(1)	340.5
2Ce(2)	437.9	1Ce(1)	332.6	1Sb(3)	353.2
2Ce(1)	445.9	1Ce(2)	337.1	1Ce(2)	386.7
Ce(2)–2Pd(1)	326.9	Pd2–2Sb(2)	268.4	Sb2–1Pd(3)	262.8
2Sb(1)	329.0	2Sb(3)	271.1	2Pd(1)	266.5
2Sb(2)	329.9	4Pd(1)	311.3	1Pd(2)	268.4
1Pd(2)	330.4	2Ce(2)	330.4	1Pd(1)	269.6
2Pd(3)	331.5	2Ce(1)	341.9	2Ce(2)	329.9
1Pd(4)	332.0			2Ce(1)	330.9
2Sb(3)	333.7	Pd3–1Sb(2)	262.8	1Ce(2)	384.6
1Pd(1)	337.1	2Sb(1)	267.2		
1Pd(3)	359.3	1Sb(1)	270.1	Sb3–2Pd(1)	270.7
1Sb(2)	384.6	1Pd(4)	276.2	2Pd(2)	271.1
1Sb(1)	386.7	2Ce(2)	331.5	4Ce(2)	333.7
1Ce(1)	437.9	2Pd(3)	354.3	2Sb(1)	353.2
2Ce(2)	445.9	1Ce(2)	359.3	2Pd(4)	381.9
1Ce(2)	472.4	2Ce(1)	366.6		
		Pd4–2Pd(3)	276.2		
		4Sb(1)	280.5		
		2Ce(2)	332.0		
		2Ce(1)	359.1		
		2Sb(3)	381.9		

[a] All distances shorter than 575 pm (Ce–Ce), 510 pm (Ce–Pd and Ce–Sb), and 400 pm (Pd–Pd, Pd–Sb, and Sb–Sb) are listed. Standard deviations are all equal to or less than 0.1 pm.

CN 20 as is typical for intermetallic compounds. Both cerium atoms have four cerium neighbors at Ce–Ce distances ranging from 437.9 to 472.4 pm. While Ce(1) possesses ten palladium and six antimony neighbors, Ce(2) has eight palladium and eight antimony neighbors. Thus both cerium positions have the same CN but different crystal chemical environments.

Each of the four different palladium atoms has CN 12. Both Pd(1) and Pd(2) have the same environment with four Ce, four Pd and four Sb in their coordination shells. However, owing to small distortions, the interatomic distances are different. The Pd–Sb distances for Pd(1) and Pd(2) range from 266.5 to 271.1 pm. They compare well with the Pd–Sb distances in $EuPd_2Sb_2$ (260.1–268.3 pm) with $CaBe_2Ge_2$-type structure [10]. The palladium neighbors are all at distances larger than 310 pm. They belong to the coordination shells but do not contribute to Pd–Pd bonding. This is different for Pd(3) and Pd(4). Both of these atoms have palladium neighbors at 276.2 pm. This distance compares well with twice the metallic radius of palladium for CN 12 of 275.2 pm [24]. For Pd(3), the four antimony neighbors have an average distance of 266.8 pm, while the four nearest antimony neighbors of Pd(4) are at the longer distance of 280.5 pm.

The antimony atoms have CN 10, CN 11 and CN 12 for Sb(2), Sb(1) and Sb(3) respectively. They have four or five nearest palladium neighbors at distances ranging from 262.8 to 280.5 pm. As discussed above, the antimony atoms possess no strong Sb–Sb interactions. For Sb(1) and Sb(3), the nearest Sb atoms are at 340.5 pm and 353.2 pm respectively. These Sb–Sb distances are significantly longer than in the structure of α-antimony, where each antimony atom has three neighbors at 290.8 pm (two-electron bonds) and three neighbors at 335.5 pm (van der Waals bonds) [27]. Furthermore, Sb(2) does not even have one antimony atom in its coordination shell.

Considering the comparisons of the interatomic distances, one may conclude that Ce–Pd, Ce–Sb and Sb–Sb bondings play only a subordinate rule in $Ce_3Pd_6Sb_5$, while Pd–Pd and Pd–Sb bondings are quite strong. The structure of $Ce_3Pd_6Sb_5$ may thus, alternatively, be described as a presumably covalently bonded three-dimensional infinite $[Pd_6Sb_5]$ polyanion in which the cerium atoms are embedded, as indicated in Fig. 2.

Table 4
Comparison of calculated and observed intensities for $Ce_3Pd_6Sb_5$

h	k	l	d_{hkl}	I_{calc}(%)	I_{exp}(%)	I_{exp}1.505
0	0	2	5.0250	6.3	5	7.5
0	0	3	3.3500	3.4		
3	0	2	3.3497	1.4	4	6
3	1	0	3.1652	9.1	7	10.5
2	0	3	2.9999	1.8		
2	1	2	2.9893	2.1	1	1.5
4	0	2	2.7990	3.4	2	3.5
3	0	3	2.6858	21.9		
0	1	3	2.6783	28.6		
3	1	2	2.6782	100	100	150.5
0	0	4	2.5125	5.6	3	4.5
2	1	3	2.4890	7.8	4	6
5	1	0	2.3072	8.6	5	7.5
3	1	3	2.3007	7.7	5	7.5
5	1	1	2.2487	8.3		
6	0	0	2.2468	26.8	20	30.1
0	2	0	2.2295	38.4	24	36.1
3	0	4	2.1930	1.1		
6	0	1	2.1927	2.2		
0	1	4	2.1889	2.6	3	4.5
5	0	3	2.1004	1.7		
4	1	3	2.0968	3.0		
5	1	2	2.0968	5.4	4	6
3	1	4	1.9679	15	8	12
3	0	5	1.8348	9.4		
0	1	5	1.8324	6.3	9	13.5
6	1	3	1.7214	10.2	6	9
3	2	3	1.7155	11.5	7	10.5
6	2	0	1.5826	17.9	6	9
3	1	6	1.4805	9.7	4	6
6	1	5	1.4200	8.2		
9	1	0	1.4199	2.5	6	9
3	2	5	1.4167	8.2	4	6
9	0	3	1.3674	3.2		
9	1	2	1.3664	5.7	4	6
0	3	3	1.3586	3.6		
3	3	2	1.3586	12.4	7	10.5

[a] Indicates peaks which overlap. Owing to overlap with the 100% intensity peak, a rescaling of the observed intensity is also given, on the basis of the sum of the overlapping intensities.

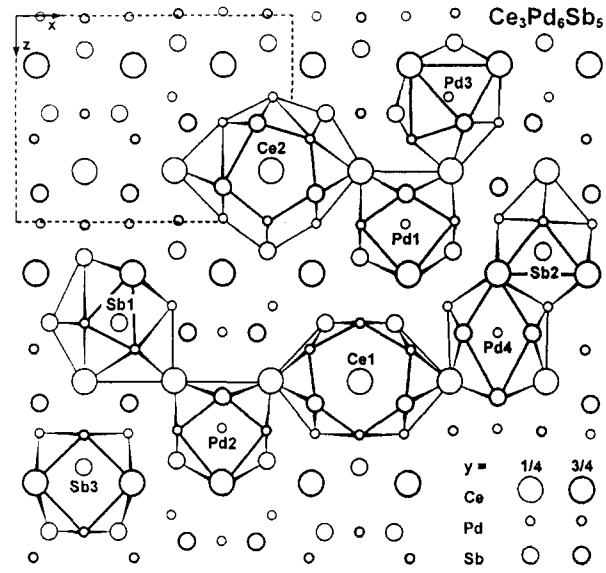

Fig. 1. Crystal structure and coordination polyhedra of $Ce_3Pd_6Sb_5$. All atoms are situated on mirror planes at $y = \frac{1}{4}$ and $y = \frac{3}{4}$ respectively indicated by thin and thick lines.

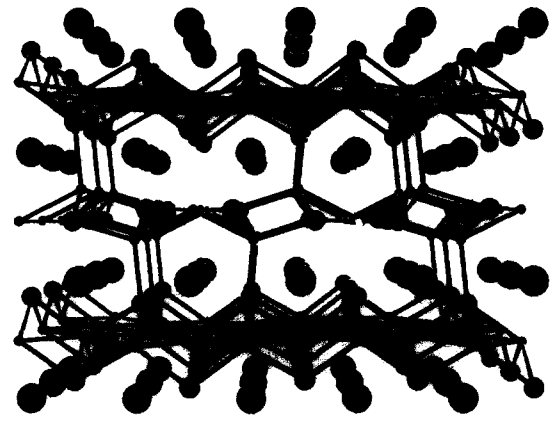

Fig. 2. Perspective view of the $Ce_3Pd_6Sb_5$ structure along the y direction [21]. The three-dimensionally infinite Pd_6Sb_5 polyanion is outlined.

3.2. Magnetic properties

The inverse of the magnetic susceptibility as a function of temperature is shown in Fig. 4. The inset to Fig. 4 is the susceptibility from 4.2 to 30 K which clearly shows an antiferromagnetic transition at 6.0(1) K. There is an obvious difference in χ^{-1} between the cooling and warming data with several breaks in the cooling curve as the loose powder reorients in the magnetic field. An anisotropic environment around the rare earth can lead to an anisotropy in the moment via interaction of the moment with the crystal field and spin–orbit coupling. If large enough, this anisotropy will produce a torque on small crystalline particles and force them to reorient so that the maximum moment is parallel to the applied field. Since the $Ce_3Pd_6Sb_5$ powder used for measurement was obtained from a polycrystalline sample, complete orientation of all single-crystal grains is not assured. Given that the warming data do not exhibit the vertical discontinuities present in the cooling data, the orientation of the powder remains fixed on heating. The apparent anisotropy is at least 14% from a comparison of heating data with the initial randomly oriented powder at 295 K.

Only data above 125 K, collected on warming, was used in fitting to a Curie–Weiss expression $\chi = \chi_0 + C/(T - \theta)$. Deviations from Curie behavior below this temperature are presumably due to crystal field effects. The observed moment (per cerium) of $2.67(6)\mu_B$ is consistent with trivalent cerium. The apparent exchange constant θ determined from a simple linear extrapolation of χ^{-1} for the cooling data above 200 K

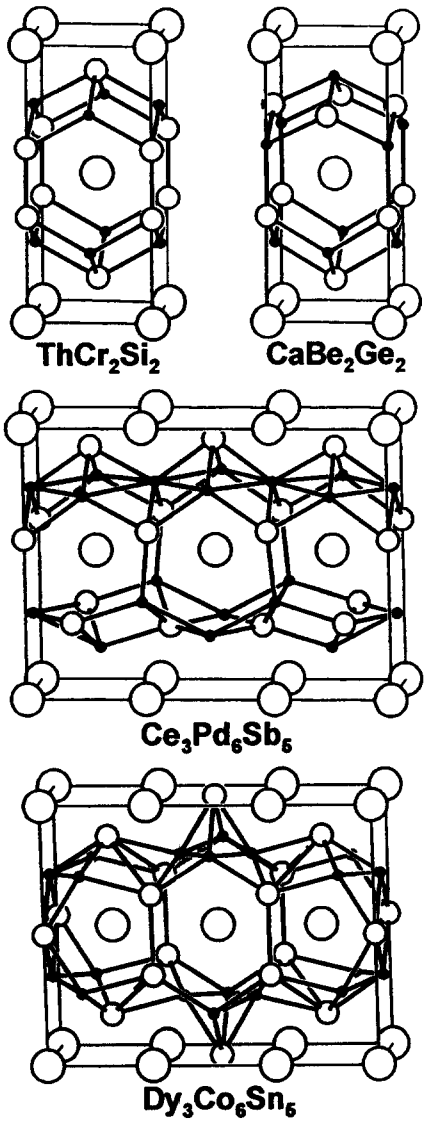

Fig. 3. Crystal chemical relationship between the structures of $ThCr_2Si_2$, $CaBe_2Ge_2$, $Ce_3Pd_6Sb_5$ and $Dy_3Co_6Sn_5$. The origins of the $CaBe_2Ge_2$ and $Ce_3Pd_6Sb_5$ structures are shifted for better comparison with the other structures.

is approximately −19 K (antiferromagnetic, with a smaller moment of $2.56\mu_B$), while θ found by fitting the warming data between 125 and 300 K is 6 ± 4 K. A positive Weiss constant would appear to indicate ferromagnetic exchange; yet $Ce_3Pd_6Sb_5$ orders antiferromagnetically with a Néel temperature of 6.0(1) K. This may indicate that the dominant antiferromagnetic exchange does not lie in the direction of maximum moment. We also note that since, for $T \geq \Delta/k_B$ (Δ is a crystal field splitting energy), the magnetic susceptibility for a free ion can be fitted to a Curie–Weiss curve [28], the θ value of 6 K for the warming curve may also indicate that the high temperature Weiss constant may have contributions from both exchange and crystal field effects. In such a case, care must be

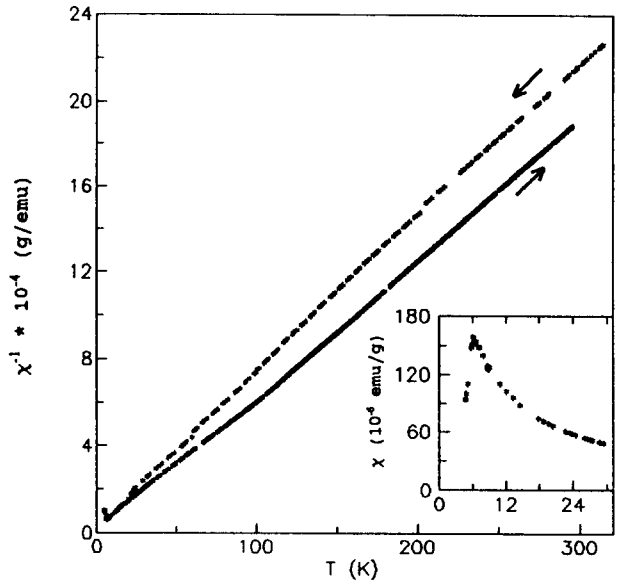

Fig. 4. Inverse magnetic susceptibility as a function of temperature between 4.2 K and 300 K for $Ce_3Pd_6Sb_5$. Inset shows the magnetic susceptibility from 4.2 to 30 K.

taken in interpreting small θ values, particularly when both effects have anisotropic components.

3.3. Resistance

With cracks present in the sample, only an upper bound may be placed on the absolute resistivity. This upper bound is calculated to be 3.3 mΩ cm at 295 K, which is about an order of magnitude larger than typical intermetallic compounds without cracks but is, in fact, comparable with the observed resistivity of CePdSb (4 mΩ cm at 295 K [7]). The temperature dependence of the relative resistance, however, is revealing. No propagation of cracks, evident as discontinuities or hysteresis in the data was observed. Fig. 5 shows the normalized resistance of $Ce_3Pd_6Sb_5$ from 4.2 to 295 K. Features worthy of note are the broad region of negative curvature roughly centered at 125 K, a broad minimum near 17 K and an abrupt change in slope near 6 K. The feature at 6 K is most easily explained as due to the antiferromagnetic ordering. The broad region may be attributed to the effects of interactions between the conduction electrons and localized f electrons in a crystal field [29] as the occupancy of the crystal field levels changes with temperature. Similar behavior was observed in CePdSn ($T_N = 7.5$ K) [7,29]. A broad minimum was also observed for CePdSn and it was suggested [7] that it may be due to the presence of some Kondo-like interactions. Kondo-like interactions may also be occurring in $Ce_3Pd_6Sb_5$, but an explanation of increased scattering due to increased magnetic fluctuations as

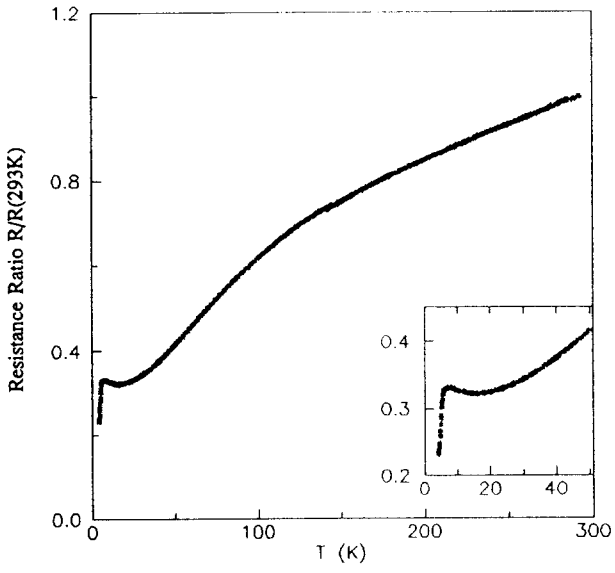

Fig. 5. Normalized resistance for $Ce_3Pd_6Sb_5$ between 4.2 and 300 K. The upper bound on the resistivity at 295 K is 3.3 mΩ cm.

one approaches the ordering temperature is also feasible.

4. Conclusions

We have prepared and studied the crystal structure, magnetic and electrical properties on the new ternary antimonide $Ce_3Pd_6Sb_5$. The structure of this material is of a new type. Unlike $Dy_3Co_6Sn_5$, which is derived from the $ThCr_2Si_2$ structure, $Ce_3Pd_6Sb_5$ is related instead to the $CaBe_2Ge_2$ structure type to which $CePd_2Sb_2$ belongs. Metallic $Ce_3Pd_6Sn_5$ orders antiferromagnetically at 6.0(1) K. From the magnetic susceptibility, we conclude that the cerium moments are moderately anisotropic with a high temperature value of $2.67(6)\mu_B$ and are therefore attributed to trivalent cerium. The resistance also shows the effects of antiferromagnetic ordering and of some crystal field interactions of moderate strength. A minimum in the resistance near 17 K may also suggest some Kondo interactions in $Ce_3Pd_6Sb_5$.

5. Acknowledgments

We are grateful to Professor A. Simon for the use of the research facilities at the Max-Planck-Institut. We would like to acknowledge the support of the Office of Naval Research and the Stiftung Stipendienfonds des Verbandes der Chemischen Industrie for a Liebig grant to R.P. Special thanks go to W. Röthenbach for the Guiner powder patterns and N.E. Brese for some useful advice.

References

[1] Z. Fisk, D.W. Hess, C.J. Pethick, D. Pines, J.L. Smith, J.D. Thompson and J.O. Willis, *Science, 239* (1988) 33–42.
[2] M. Loewenhaupt and K.H. Fischer, in K.A. Gschneider, Jr., and L. Eyring (eds.), *Handbook on the Chemistry and Physics of Rare Earths*, Vol. 16, Elsevier, Amsterdam, 1993, Chapter 105.
[3] F. Steglich, C. Geibel, K. Gloos, G. Olesch, C. Schank, C. Wassilew, A. Loidl, A. Krimmel and G.R. Stewart, *J. Low Temp. Phys., 95* (1–2) (1994) 3–22.
[4] R.A. Gordon, Y. Ijiri, C.M. Spencer and F.J. DiSalvo, *J. Alloys Comp.*, in press.
[5] R. Pöttgen, *J. Mater Chem.*, submitted.
[6] R. Pöttgen, H. Borrmann and R.K. Kremer, *J. Magn. Magn. Mater.*, submitted.
[7] S.K. Malik and D.T. Adroja, in G. Oomi et al. (eds.), *Transport and Thermal Properties of f-Electron systems*, Plenum, New York, 1993, pp. 55–70.
[8] B.D. Rainford, D.T. Adroja and J.M.E. Geers, *Physica B, 199–200* (1994) 556–557.
[9] R. Marazza, D. Rossi and R. Ferro, *J. Less-Common Met.*, 75 (1980) P25–P28.
[10] W.K. Hofmann and W. Jeitschko, *Monatsh. Chem., 116* (1985) 569–580.
[11] O. Sologub, K. Hiebl, P. Rogl, H. Noël and O. Bodak, *J. Alloys Comp., 210* (1994) 153–157.
[12] W. Jeitschko, private communication, 1995.
[13] J.P. Kappler, M.J. Besnus, P. Lehmann, A. Meyer and J. Sereni, *J. Less-Common Met., 111* (1985) 261–264.
[14] H. Sthioul, D. Jaccard and J. Sierro, in P. Wachter and H. Boppart (eds.), *Valence Instabilities*, North-Holland, Amsterdam, 1982, pp. 443–445.
[15] P.E. Werner, L. Eriksson and M. Westdahl, *J. Appl. Crystallogr., 18* (1985) 367.
[16] K. Yvon, W. Jeitschko and E. Parthé, *J. Appl. Crystallogr., 10* (1977) 73.
[17] G.M. Sheldrick, SHELX-86, Program for the Solution of Crystal Structures, University of Göttingen, Göttingen, 1986.
[18] G.M. Sheldrick, SHELX-93, Program for Crystal Structure Refinement, University of Göttingen, Göttingen, 1993.
[19] Z. Ban and M. Sikirica, *Z. Anorg. Allg. Chem., 356* (1967), 96.
[20] B. Eisenmann, N. May, W. Müller and H. Schäfer, *Z. Naturforsch., 27b* (1972) 1155.
[21] E. Keller, SCHAKAL 92, Kristallographisches Institut, Universität Freiburg, Freiburg, 1993.
[22] R. Pöttgen, *Z. Naturforsch. b*, in press.
[23] R. Pöttgen, *J. Alloys Comp.*, in press.
[24] E. Teatum, K.A. Gschneider, Jr., and J. Waber, *Rep. LA-2345*, 1960 (US Department of Commerce, Washington, DC).
[25] W.K. Hofmann and W. Jeitschko, *J. Less-Common Met., 138* (1988) 313–322.
[26] V.K. Pecharskii, Yu.V. Pankevich and O.I. Bodak, *Dopov. Akad. Nauk Ukr. RSR, Ser. B: Geol., Geofiz. Khim. Biol. Nauki, (4)* (1982) 44–48.
[27] J. Donohue, *The Structures of the Elements*, Wiley, New York, 1974.
[28] W.E. Hatfield, in A.K. Cheetham and P. Day (eds.), *Solid State Chemistry: Techniques*, Oxford University Press, Oxford, 1987, Chapter 4.
[29] S.K. Malik, D.T. Adroja, S.K. Dhar, R. Vijayaraghavan and B.D. Padalia, *Phys. Rev. B, 40(4)* (1989) 2414–2418.